A Hierarchical Patch-Enhanced Framework for the Accurate Segmentation of Oral Squamous Cell Carcinoma in Histopathological Images

Vinaya R. Kundatarkar
Department of Computer Science and Engineering, Dayananda Sagar College of Engineering, Visvesvaraya Technological University, Bengaluru, Karnataka, India
vinayar_12@rediffmail.com (corresponding author)

Annapurna P. Patil
Department of Information Science and Engineering, Dayananda Sagar College of Engineering, Visvesvaraya Technological University, Bengaluru, Karnataka, India
annapurnap2@gmail.com

Savitha K. Shetty
Department of Information Technology, Ramaiah Institute of Technology, Visvesvaraya Technological University, Bengaluru, Karnataka, India
savita_ks1@msrit.edu

Received: 15 March 2026 | Revised: 22 April 2026 | Accepted: 30 April 2026

 DOI: https://doi.org/10.48084/etasr.18746

ABSTRACT

An early diagnosis of oral squamous cell carcinoma is a critical step in improving patient survival, but manual histopathological tests are still slow, labor-intensive, and subject to expert opinions. Deep learning has been applied to automated analysis of cancer, although current models have difficulties in the multi-scale and complexity of oral tumor tissue epithelia. To overcome this, this study introduces a new Hierarchical Patch-Enhanced Framework (HPEF) combining multi-scale feature extraction, multi-scale progressive knowledge distillation, and adaptive attention to achieve precise segmentation of malignant epithelial segments. In-depth experiments on two publicly available histopathological datasets, ORCA and OCDC, showed that the proposed HPEF achieved accuracy scores of 0.923 and 0.978, Dice scores of 0.878 and 0.967, and Intersection-over-Union (IoU) scores of 0.735 and 0.943, respectively, which are significantly higher than state-of-the-art CNN-based, Transformer-based, and hybrid segmentation models. These findings indicate that HPEF has the potential to be a reliable instrument to help pathologists screen early cases of oral cancer.

Keywords-oral squamous cell carcinoma; hierarchical patch-enhanced framework; multi-scale feature extraction; knowledge distillation; attention-based segmentation

I. INTRODUCTION

Cancer is characterized by uncontrolled proliferation of abnormal cells that invade surrounding tissues and may metastasize to distant organs. Oral cancer is a major global health concern that affects various regions of the oral cavity, including the lips, tongue, gingiva, and buccal mucosa. Among oral malignancies, Oral Squamous Cell Carcinoma (OSCC) accounts for more than 90% of all cases and remains one of the most prevalent cancers in South Asian countries. According to global cancer statistics, hundreds of thousands of new cases of oral cancer are diagnosed every year, with a high mortality rate due to late diagnosis [1]. Histopathological examination of biopsy samples is considered the gold standard for OSCC diagnosis; however, manual microscopic analysis is time-consuming and dependent on the expertise of pathologists [2].

Recent advances in artificial intelligence and deep learning have enabled automated analysis of histopathological images, improving diagnostic accuracy and efficiency in cancer detection tasks. Clinically, OSCC is usually a non-healing sore or ulcer of the mouth, usually accompanied by pain or bleeding, difficulty chewing or swallowing, swelling of the jaw, and speech impairment [3]. Several risk factors lead to its development, including tobacco chewing, heavy alcohol use, Human Papillomavirus (HPV) infection, genetic predisposition, and local lifestyle habits. Despite advances in treatment, OSCC remains associated with a low survival rate of about 50%,

which highlights the urgency of efficient and prompt diagnosis [4]. Microscopic examination through a microscope on biopsy samples still remains the gold standard in the detection of OSCC [5].

The increasing prevalence of OSCC and its relatively low survival rate highlight the need for accurate and early diagnostic methods [6]. The main contributions of this work are summarized as follows:

- A novel Hierarchical Patch-Enhanced Framework (HPEF) designed for accurate segmentation of OSCC in histopathological images.
- A master-slave knowledge distillation mechanism, enabling effective transfer of global contextual information and fine-grained cellular features.
- An adaptive hierarchical attention module that enhances communication between region-level and pixel-level representations.
- Extensive evaluation on ORCA and OCDC datasets demonstrates superior performance compared to state-of-the-art CNN and transformer-based segmentation models.

Unlike existing CNN-based and Transformer-based segmentation frameworks that primarily focus on single-scale feature extraction or independent attention mechanisms, the HPEF introduces a joint multi-scale learning paradigm integrating scale-adaptive knowledge distillation and hierarchical attention modeling. Table I highlights that existing approaches either focus on single-scale representations, lack efficient knowledge transfer mechanisms, or fail to model hierarchical contextual relationships, motivating the design of the proposed HPEF framework.

In [7], a CNN-based classification model was reliable even in the case of small-sized histological patches, although its efficiency was lower on borderline or suspicious lesions. In [8], the Intelligent Deep Learning Enabled OSCC Detection and Classification (IDL-OSCDC) framework demonstrated high precision-recall in various datasets. In [9], EfficientNet-B3 was employed to detect OSCC, which was relatively stable in extrapolating to rarely seen samples and avoiding overfitting in the validation stage. In [10], the Modified Gorilla Troops Optimizer (MTGO) for deep learning achieved better feature transformation and better accuracy in both training and validation contexts, but was very time-consuming since it used an iterative optimization method. In addition to single-modality analysis, multimodal approaches have been increasingly promising. In [11], an explainable Artificial Intelligence (XAI) framework was designed to orchestrate multimodal and longitudinal medical imaging data, allowing clinicians to interpret AI predictions through adaptive, hierarchical, and uncertainty-aware explainability mechanisms to improve the usability of AI systems in clinical workflows.

In [12], a systematic review of deep learning-based semantic segmentation approaches for histopathological images focused on breast, colon, and prostate cancers. This study analyzed research published between 2015 and 2024 following PRISMA guidelines and identified major trends in segmentation architectures used for cancer diagnosis and grading. In [13], recent deep learning approaches for nucleus segmentation in histopathology images were reviewed, reporting that architectures such as U-Net and its variants have shown strong performance in detecting and segmenting nuclei. In [14], the DSLVI-OCLSC model for oral carcinoma detection combined Wiener filtering, ShuffleNetV2 feature extraction, MA-CNN-BiLSTM classification, and U-Net3+ segmentation with SCA-based hyperparameter tuning, achieving 98.47% accuracy on oral cancer image datasets. In [15], an EfficientNetB3-based CNN framework for automated classification of breast cancer histopathological images achieved 92.33% accuracy on the BreaKHis dataset and employed Grad-CAM for interpretable localization of malignant regions.

TABLE I. COMPARISON OF RECENT OSCC AND HISTOPATHOLOGY-BASED METHODS

Study	Technique	Strength	Limitation
[9]	EfficientNet-based CNN	Strong generalization and reduced overfitting	Lacks multi-scale contextual feature modeling
[11]	XAI + Multimodal learning	Provides interpretability and uncertainty awareness	Not designed for pixel-level segmentation tasks
[13]	Survey on nucleus segmentation	Highlights the effectiveness of deep learning models	Focus limited to nucleus-level segmentation only
[14]	Hybrid DL segmentation framework	High accuracy with integrated preprocessing and segmentation	High computational complexity and limited cross-scale learning

II. METHODOLOGY

This section presents the proposed HPEF for OSCC segmentation. Recent studies have demonstrated the effectiveness of deep learning approaches for automatic detection and classification of OSCC from histopathological images [16].

A. Patch Generation and Regional Feature Formation

Each WSI is divided into non-overlapping 256×256×3 patches at two magnification levels (20× and 5×). Pretrained expert encoders extract patch-level features from both scales. Multi-scale representations are widely used in histopathological image analysis to capture both local cellular structures and global tissue context [17].

B. Scale-Adaptive Knowledge Distillation (SAKD)

The SAKD module is designed to bridge the semantic gap between low-resolution and high-resolution representations by transferring discriminative knowledge across magnification levels. Let G_C denote a pretrained patch encoder. For a given region k, feature representations at 5× and 20× magnifications are obtained by aggregating patch-level embeddings, as defined in (1) and (2). Specifically, $T_k^{5\times}$ represents the coarse-scale regional embedding derived from 16 patches, whereas $T_k^{20\times}$ denotes the fine-scale representation constructed from 256 high-resolution patches. Here, $t_{k,l}$ refers to the l-th patch within

region k. This formulation enables explicit modeling of both global tissue structure and local cellular morphology.

$$T_k^{5\times} = G_C(\{t_{k,1}^{5\times}, \dots, t_{k,16}^{5\times}\}) \quad (1)$$

$$T_k^{20\times} = G_C(\{t_{k,1}^{20\times}, \dots, t_{k,256}^{20\times}\}) \quad (2)$$

where $t_{k,l}$ denotes the l-th patch within region k.

To facilitate effective cross-scale semantic alignment, a learnable token is prepended to the 5× input sequence, as shown in (3). This token acts as a semantic anchor, guiding the low-resolution pathway to adapt its representations using information distilled from the richer 20× features.

$$T_k^{5\times} = \{[tok], T_k^{5\times}\} \quad (3)$$

During training, random masking with a ratio of 0.5 is applied independently to both magnification streams, producing masked regional inputs $O_k^{5\times}$ and $O_k^{20\times}$, described by:

$$O_k^{5\times} = \{o_{k,1}^{5\times}, \dots, o_{k,16}^{5\times}\} \quad (4)$$

$$O_k^{20\times} = \{o_{k,1}^{20\times}, \dots, o_{k,256}^{20\times}\} \quad (5)$$

The master model V processes the unmasked inputs and produces class tokens E_V and patch tokens R_V, which serve as stable supervision targets. Consistency between the master and slave outputs is enforced using a cross-entropy loss defined as

$$Loss(a_u, a_v) = -\sum_i r_V^{(i)} \log r_U^{(i)} \quad (6)$$

where r_V and r_U denote the softmax-normalized probability distributions generated by the master and slave networks, respectively. The class-token loss aligns global semantic representations across magnifications, ensuring that each slave class token matches its corresponding master token at both 5× and 20× scales [18]. These two components are combined to form the overall SAKD objective:

$$Loss_{SAKD} = Loss_{CT} + Loss_{PT} \quad (7)$$

Finally, the parameters of the master network are updated using an Exponential Moving Average (EMA) of the slave network weights.

C. Collaborative Knowledge Distillation (CKD)

The CKD module complements SAKD by introducing an additional expert network trained exclusively on high-resolution (20×) patches to improve regional semantic consistency. Let G_D denote the high-resolution expert model and $R_U^{20\times}$ represent the patch tokens generated by the slave network. Knowledge transfer is defined using a cosine similarity loss:

$$CKD = 1 - \cos\left(G_D(T_k^{20\times}), R_U^{20\times}\right) \quad (8)$$

This loss encourages alignment between the expert and slave feature embeddings, promoting consistent high-resolution representations.

D. Hierarchical Multi-Scale Attention (MLHA)

The MLHA module integrates local cellular details with global tissue context across magnification scales [19]. It consists of two stages: Local Multi-Scale Attention (LMSA) and Global Multi-Scale Attention (GMSA). LMSA fuses coarse-scale (5×) and fine-scale (20×) patch tokens. Using $R_{5\times}$ as queries and $R_{20\times}$ as keys and values, the module refines low-resolution features with detailed cellular information while preserving regional spatial relationships. After regional fusion, GMSA models long-range dependencies across regions in the Whole-Slide Image (WSI), capturing global tissue architecture. For the master and slave networks, hierarchical representations are computed as:

$$MultiScale_V = GMSA(LMSA(R_V^{5\times}, R_V^{20\times}), R_V^{20\times}) \quad (9)$$

$$MultiScale_U = GMSA(LMSA(R_U^{5\times}, R_U^{20\times}), R_U^{20\times}) \quad (10)$$

To align these representations, a cosine similarity loss is applied:

$$MLHA = 1 - \cos\left(MultiScale_V, MultiScale_U\right) \quad (11)$$

Finally, the overall training objective combines all components:

$$Loss_{final} = Loss_{SAKD} + CKD + MLHA \quad (12)$$

This joint optimization enables effective cross-scale knowledge transfer, expert-guided feature refinement, and hierarchical contextual modeling, improving segmentation accuracy in OSCC histopathology images.

III. EXPERIMENTAL SETUP AND RESULTS

Two publicly available H&E-stained histopathological datasets, ORCA [20, 21] and OCDC [22, 23], were used to evaluate the proposed model. The ORCA dataset, derived from The Cancer Genome Atlas (TCGA), contains 200 WSIs captured at 40× magnification with a resolution of 4500×4500 pixels. The OCDC dataset consists of 1,020 histopathological images of size 640×640 pixels, collected from OSCC patients at the Federal University of Uberlândia. This dataset has been widely used for evaluating segmentation models in oral cancer histopathology.

Figure 1 illustrates representative histopathological images, corresponding tumor masks, and highlighted tumor regions used in this study. The datasets were divided into 70% training, 15% validation, and 15% testing subsets to ensure reliable performance evaluation. All experiments were implemented using Python and PyTorch on a workstation equipped with an NVIDIA RTX 3080 GPU with 24 GB memory.

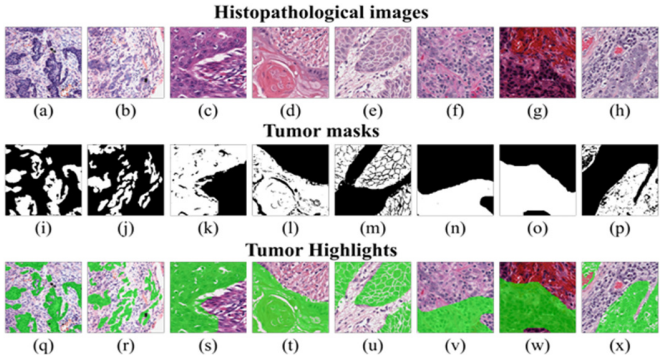

Fig. 1. Histopathological images, tumor masks, and tumor-highlighted regions.

A. Results

The performance of the proposed HPEF was evaluated on ORCA and OCDC using standard segmentation metrics, including Accuracy, Intersection-over-Union (IoU), and Dice coefficient. Figure 2 illustrates the comparative performance of the proposed model against several state-of-the-art CNN-based and Transformer-based architectures on the ORCA dataset, while Table II summarizes the corresponding quantitative results. The proposed model achieves an improvement of approximately 6–7% in Dice score and IoU compared to the strongest baseline models.

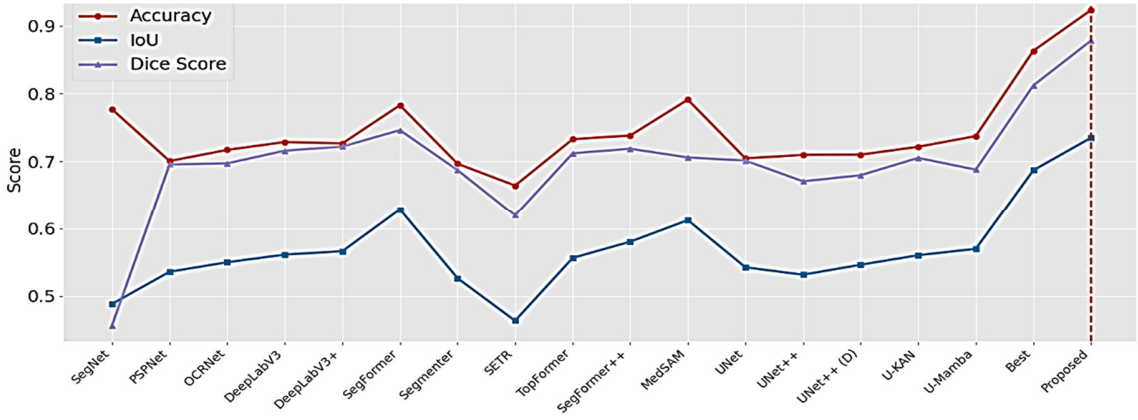

Fig. 2. ORCA dataset: Accuracy, IoU, and Dice score comparison.

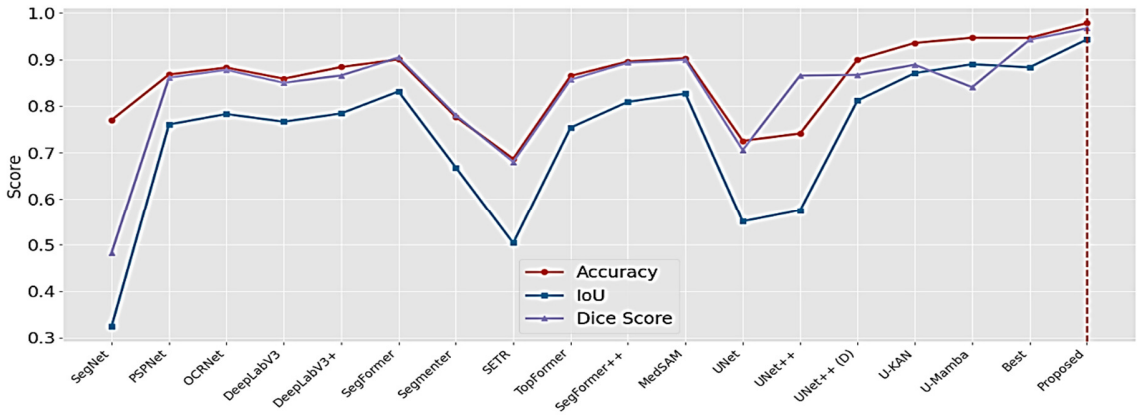

Fig. 3. OCDC dataset: Accuracy, IoU, and Dice score comparison.

TABLE II. QUANTITATIVE COMPARISON ON ORCA

Model	Accuracy	Dice score	IoU
SegNet	0.7771	0.4562	0.4881
PSPNet	0.7008	0.6958	0.5358
OCRNet	0.7172	0.6973	0.5499
DeepLabV3	0.7288	0.7161	0.5612
DeepLabV3+	0.7267	0.7221	0.5663
SegFormer	0.7830	0.7463	0.6286
Segmenter	0.6968	0.6874	0.5263
SETR	0.6646	0.6201	0.4632
TopFormer	0.7330	0.7122	0.5563
SegFormer++	0.7384	0.7189	0.5804
MedSAM Adapter	0.7912	0.7061	0.6124
UNet	0.7047	0.7015	0.5424
UNet++	0.7099	0.6709	0.5314
UNet++ (Dense)	0.7102	0.6799	0.5462
U-KAN	0.7218	0.7054	0.5603
U-Mamba	0.7375	0.6881	0.5698
Table Best (ORCA)	**0.8631**	**0.8121**	**0.6872**
Proposed HPEF	**0.9230**	**0.8780**	**0.7350**

TABLE III. QUANTITATIVE COMPARISON ON OCDC

Model	Accuracy	Dice score	IoU
SegNet	0.7699	0.4830	0.3246
PSPNet	0.8677	0.8611	0.7603
OCRNet	0.8826	0.8777	0.7828
DeepLabV3	0.8586	0.8500	0.7662
DeepLabV3+	0.8837	0.8657	0.7840
SegFormer	0.9001	0.9042	0.8312
Segmenter	0.7766	0.7800	0.6677
SETR	0.6866	0.6800	0.5039
TopFormer	0.8646	0.8566	0.7535
SegFormer++	0.8958	0.8932	0.8090
MedSAM Adapter	0.9026	0.8994	0.8267
UNet	0.7251	0.7054	0.5507
UNet++	0.7409	0.8654	0.5749
UNet++ (Dense)	0.8995	0.8668	0.8116
U-KAN	0.9351	0.8886	0.8708
U-Mamba	0.9466	0.8404	0.8897
Table Best (OCDC)	**0.9463**	**0.9424**	**0.8831**
Proposed HPEF	**0.9780**	**0.9670**	**0.9430**

Figure 3 presents the performance evaluation on the OCDC dataset, with detailed quantitative comparisons provided in Table III. The proposed HPEF model achieves an accuracy of 0.978, IoU of 0.943, and Dice score of 0.967, outperforming all baseline methods. Notably, the improvement over the strongest baseline models is evident, with gains of approximately 1.8% in accuracy and 6–7% in IoU, highlighting the robustness of the proposed method across different datasets. The model demonstrates consistent generalization across datasets with significant gains in segmentation accuracy and overlap metrics. All baseline models were evaluated under identical experimental settings to ensure a fair and unbiased comparison.

IV. CONCLUSION

This study proposes a hierarchical patch-enhanced system for automated segmentation of OSCC in histopathological images. The multi-scale feature extraction strategy and master-slave distillation strategy yield a very successful combination of the broad tissue organization and the finer cellular features that are important in identifying malignant epithelial regions. The adaptive attention mechanism also enhances the awareness of boundaries, leading to greater performance in the segmentation of various tissue structures. Large-scale testing with the ORCA and OCDC datasets shows that the proposed model exhibits greater accuracy and better boundary precision than a variety of popular deep learning baselines by a significant margin, demonstrating its effectiveness for real-world clinical deployment.

Subsequent research will discuss whole-slide processing extensions and combining multi-modal diagnostic cues to enhance the clinical applicability even further. The proposed framework demonstrates strong potential for computer-assisted oral cancer diagnosis and may serve as a reliable tool to support pathologists in clinical decision-making.

DECLARATION OF COMPETING INTERESTS

The authors declare that they have no known competing financial interests or personal relationships that could have appeared to influence the work reported in this paper.

ACKNOWLEDGMENT

This research received no specific grant from any funding agency in the public, commercial, or not-for-profit sectors.

DATA AVAILABILITY

The datasets used in this study are publicly available. The ORCA dataset is derived from The Cancer Genome Atlas (TCGA) and is available at [21], and the OCDC dataset is available at [23].

REFERENCES

[1] F. Bray *et al.*, "Global cancer statistics 2022: GLOBOCAN estimates of incidence and mortality worldwide for 36 cancers in 185 countries," *CA: A Cancer Journal for Clinicians*, vol. 74, no. 3, pp. 229–263, May 2024, https://doi.org/10.3322/caac.21834.

[2] I. U. Haq, M. Ahmed, M. Assam, Y. Y. Ghadi, and A. Algarni, "Unveiling the Future of Oral Squamous Cell Carcinoma Diagnosis: An Innovative Hybrid AI Approach for Accurate Histopathological Image Analysis," *IEEE Access*, vol. 11, pp. 118281–118290, 2023, https://doi.org/10.1109/ACCESS.2023.3326152.

[3] E. Natarajan, "Oral and Oropharyngeal Cancer," in *Dental Science for the Medical Professional*, C. E. Niekrash, E. M. Ferneini, and M. T. Goupil, Eds. Springer International Publishing, 2023, pp. 261–301.

[4] M. F. Kabir, M. Y. Ahmad, R. Uddin, M. Cordero, and S. Kant, "Accurate and lightweight oral cancer detection using SE-MobileViT on clinically validated image dataset," *Discover Artificial Intelligence*, vol. 5, no. 1, July 2025, Art. no. 173, https://doi.org/10.1007/s44163-025-00442-2.

[5] D. Menditti *et al.*, "Personalized Medicine in Oral Oncology: Imaging Methods and Biological Markers to Support Diagnosis of Oral Squamous Cell Carcinoma (OSCC): A Narrative Literature Review," *Journal of Personalized Medicine*, vol. 13, no. 9, Sept. 2023, Art. no. 1397, https://doi.org/10.3390/jpm13091397.

[6] M. Á. González-Moles, M. Aguilar-Ruiz, and P. Ramos-García, "Challenges in the Early Diagnosis of Oral Cancer, Evidence Gaps and Strategies for Improvement: A Scoping Review of Systematic Reviews," *Cancers*, vol. 14, no. 19, Oct. 2022, Art. no. 4967, https://doi.org/10.3390/cancers14194967.

[7] K. Oya, K. Kokomoto, K. Nozaki, and S. Toyosawa, "Oral squamous cell carcinoma diagnosis in digitized histological images using convolutional neural network," *Journal of Dental Sciences*, vol. 18, no. 1, pp. 322–329, Jan. 2023, https://doi.org/10.1016/j.jds.2022.08.017.

[8] A. A. Alanazi, M. M. Khayyat, M. M. Khayyat, B. M. Elamin Elnaim, and S. Abdel-Khalek, "Intelligent Deep Learning Enabled Oral Squamous Cell Carcinoma Detection and Classification Using Biomedical Images," *Computational Intelligence and Neuroscience*, vol. 2022, pp. 1–11, June 2022, https://doi.org/10.1155/2022/7643967.

[9] E. Albalawi *et al.*, "Oral squamous cell carcinoma detection using EfficientNet on histopathological images," *Frontiers in Medicine*, vol. 10, Jan. 2024, https://doi.org/10.3389/fmed.2023.1349336.

[10] B. Ananthakrishnan, A. Shaik, S. Kumar, S. O. Narendran, K. Mattu, and M. S. Kavitha, "Automated Detection and Classification of Oral Squamous Cell Carcinoma Using Deep Neural Networks," *Diagnostics*, vol. 13, no. 5, Feb. 2023, Art. no. 918, https://doi.org/10.3390/diagnostics13050918.

[11] A. P. De Mortanges *et al.*, "Orchestrating explainable artificial intelligence for multimodal and longitudinal data in medical imaging," *npj Digital Medicine*, vol. 7, no. 1, July 2024, Art. no. 195, https://doi.org/10.1038/s41746-024-01190-w.

[12] D. I. T. M. H. Tan, X. J. Tan, L. L. Lim, K. S. Ab Rahman, and J. J. W. Siet, "A systematic review of semantic segmentation methods for histopathology images: a focused survey on breast, colon, and prostate cancers," *Applied Intelligence*, vol. 55, no. 16, Oct. 2025, Art. no. 1036, https://doi.org/10.1007/s10489-025-06906-3.

[13] A. Basu, P. Senapati, M. Deb, R. Rai, and K. G. Dhal, "A survey on recent trends in deep learning for nucleus segmentation from histopathology images," *Evolving Systems*, vol. 15, no. 1, pp. 203–248, Feb. 2024, https://doi.org/10.1007/s12530-023-09491-3.

[14] A. A. Alzahrani *et al.*, "Deep structured learning with vision intelligence for oral carcinoma lesion segmentation and classification using medical imaging," *Scientific Reports*, vol. 15, no. 1, Feb. 2025, Art. no. 6610, https://doi.org/10.1038/s41598-025-89971-5.

[15] O. Al-Omari, O. Alkhatib, and T. Al-Omari, "CNN-Based Automated Detection of Metastatic Cancer in Histopathology Images," *Engineering, Technology & Applied Science Research*, vol. 15, no. 4, pp. 24478–24485, Aug. 2025, https://doi.org/10.48084/etasr.10888.

[16] M. Das, R. Dash, S. Kumar Mishra, and A. Kumar Dalai, "An Ensemble Deep Learning Model for Oral Squamous Cell Carcinoma Detection Using Histopathological Image Analysis," *IEEE Access*, vol. 12, pp. 127185–127197, 2024, https://doi.org/10.1109/ACCESS.2024.3450444.

[17] D. Tao *et al.*, "MCF-UNet: Multi-level context fusion unet for immunohistochemical positive cell detection," *Pattern Recognition*, vol. 179, Nov. 2026, Art. no. 113630, https://doi.org/10.1016/j.patcog.2026.113630.

[18] L. C. Chen, Y. Zhu, G. Papandreou, F. Schroff, and H. Adam, "Encoder-Decoder with Atrous Separable Convolution for Semantic Image Segmentation," presented at the Proceedings of the European Conference on Computer Vision (ECCV), 2018, pp. 801–818.

[19] A. Mathew and M. Jossy A, "Automated oral cancer detection with histopathological images using efficient deep-learning models," *Bioinspired, Biomimetic and Nanobiomaterials*, vol. 15, no. 1, pp. 4–13, Dec. 2025, https://doi.org/10.1680/jbibn.24.00010.

[20] F. Martino *et al.*, "Deep Learning-Based Pixel-Wise Lesion Segmentation on Oral Squamous Cell Carcinoma Images," *Applied Sciences*, vol. 10, no. 22, Nov. 2020, https://doi.org/10.3390/app10228285.

[21] "ORCA dataset." [Online]. Available: https://sites.google.com/unibas.it/orca.

[22] D. F. D. Dos Santos, P. R. De Faria, B. A. N. Travençolo, and M. Z. Do Nascimento, "Influence of Data Augmentation Strategies on the Segmentation of Oral Histological Images Using Fully Convolutional Neural Networks," *Journal of Digital Imaging*, vol. 36, no. 4, pp. 1608–1623, Apr. 2023, https://doi.org/10.1007/s10278-023-00814-z.

[23] D. Freire, P. Faria, A. Loyola, S. Cardoso, B. Travencolo, and M. do Nascimento, "H&E-stained oral squamous cell carcinoma histological images dataset." Mendeley Data, Dec. 28, 2022, https://doi.org/10.17632/9bsc36jyrt.1.